Main Chain and Side Chain Dynamics of the Ubiquitin Conjugating Enzyme Variant Human Mms2 in the Free and Ubiquitin-Bound States†

Leo Spyracopoulos,* Michael J. Lewis, and Linda F. Saltibus

Department of Biochemistry, University of Alberta, Edmonton, Alberta T6G 2H7, Canada

Received January 12, 2005; Revised Manuscript Received April 1, 2005

ABSTRACT: Protein ubiquitination involves a cascade of enzymatic steps where ubiquitin (Ub) is sequentially transferred as a thiolester intermediate from an E1 enzyme to an E2 enzyme and finally to the protein target with the help of a Ub−protein ligase. Protein ubiquitination brought about by the Ubc13−Mms2 (E2−E2) complex has a unique role in the cell, unrelated to protein degradation. The Mms2−Ubc13 heterodimer links Ub molecules to one another through an isopeptide bond between its own C-terminus and Lys-63 on another Ub. The role of Mms2 is to orient a target-bound Ub molecule such that its Lys-63 is proximal to the C-terminus of the Ub molecule that is covalently linked to the active site of Ubc13. To gain insight into the influence of protein dynamics on the affinity of Ub for Mms2, we have determined pico- to nanosecond time scale fluctuations of the main chain and methyl side chains of human Mms2 in the free and Ub-bound states using solution state ^{15}N and ^{2}H nuclear magnetic resonance relaxation measurements. Analysis of the relaxation data allows for a semiquantitative estimation of the conformational entropy change ($T\Delta S_{NMR}$) for the main chain and side chain methyl groups of Mms2 upon binding Ub. The value of $T\Delta S_{NMR}$ for the main chain and side chain methyl groups of Mms2 is -8 ± 2 and -2 ± 2 kcal mol^{-1}, respectively. The experimental $\Delta G_{binding}$ for the Mms2·Ub complex is -6 kcal mol^{-1}. Estimation of $\Delta G_{binding}$ using an empirical structure-based approach that does not account for changes in main chain entropy yields a value of -17 ± 2 kcal mol^{-1}. However, inclusion of $T\Delta S_{NMR}$ for the main chain of Mms2 increases the estimated $\Delta G_{binding}$ to -9 ± 3 kcal mol^{-1}. Assuming that changes in Ub main chain dynamics contribute to $T\Delta S_{NMR}$ to the same extent as Mms2, the estimated $\Delta G_{binding}$ is further reduced to -1 ± 4 kcal mol^{-1}, a value close to the experimental $\Delta G_{binding}$.

Posttranslational covalent attachment of ubiquitin (Ub)[1] to target proteins is a fundamental regulatory process in eukaryotes (for reviews, see refs *1*−*3*). Protein ubiquitination is mediated by a multicomponent pathway that involves the sequential transfer of Ub between proteins. Ultimately, polyubiquitin chain formation on a target substrate destines a protein for proteolytic degradation by the 26S proteasome, at least in the most common role for the protein ubiquitination pathway.

In the "classical" protein ubiquitination pathway, Ub molecules are covalently attached to each other through the C-terminus of one Ub and Lys-48 of a sequential Ub. Polyubiquitin chains containing a minimum of four Ub molecules are specifically recognized by the 26S proteasome and proteolytically degraded. Several lysine residues on the surface of Ub are utilized as isopeptide linkage sites for polyubiquitin chains. However, if lysine residues other than Lys-48 form isopeptide linkages, the molecular topology and biological role of the ensuing polyubiquitin chains may be distinct. For example, polyubiquitin chains linked through Lys-63 are involved in DNA repair and the NFκB signaling pathway (*4*−*7*).

Covalent linkage of polyubiquitin chains through Lys-63 is achieved through a protein heterodimer that consists of a catalytically active E2 (Ubc13) protein and an inactive E2-like protein or Uev (*8*−*10*). These proteins are similar in structure and sequence to E2 proteins, with the exception that the active site cysteine is absent, rendering Uev proteins catalytically inactive. Through X-ray crystallography (*11*), solution NMR (*12*−*14*), and ITC studies (*14*), a model has been developed for the Lys-63 linked polyubiqutination mechanism in which the Uev partner of the Uev·E2 heterodimer serves to position Lys-63 proximal to the active site cysteine of the catalytically active E2 binding partner.

Atomic resolution structures give insight into the molecular basis of the specificity of Ub·Uev interactions. However, a fundamental understanding of the underlying driving forces for these and other biomolecular interactions is lacking and generally known as the "protein docking problem" (*15*−*17*). For known structures, the free energy of association for a protein−protein interaction can be predicted using molecular mechanics methods that employ empirical force fields (*17*,

† This work was supported by the Canadian Institutes of Health Research (CIHR) and the Alberta Heritage Foundation for Medical Research (AHFMR). L.S. is an AHFMR Medical Research Scholar.

* To whom correspondence should be addressed. E-mail: leo.spyracopoulos@ualberta.ca. Phone: (780) 492-2417. Fax: (780) 492-0886.

[1] Abbreviations: Ub, ubiquitin; E1, Ub activating enzyme; E2 or Ubc, Ub conjugating enzyme; E3, protein−Ub ligase; Uev, Ub conjugating enzyme variant; NMR, nuclear magnetic resonance; S^2, main chain order parameter; S^2_{axis}, methyl symmetry axis order parameter; GST, glutathione *S*-transferase; DSS, 2,2-dimethyl-2-silapentane-5-sulfonic acid; HSQC, heteronuclear single-quantum coherence; NOE, nuclear Overhauser effect; AIC, Akaike's information criteria; ASA, accessible surface area.

10.1021/bi050065k CCC: $30.25
Published on Web 05/25/2005

18). These types of calculations are often limited to a single conformation of the protein−protein complex to minimize computational burden. An alternative, widespread approach is to use structure-based methods that correlate the free energy of association for a protein−protein complex with changes in ASA upon binding (*19*). As pointed out by Elcock et al., structure-based methods can be valuable if care is taken to account for various contributions to the model describing the energetics (*17*). For example, failure to account for changes in protein main chain entropy for binding of a cognate peptide to the C-domain from the protein troponin-C results in a structure-based K_D that is too low (*20*). Inclusion of changes in main chain entropy, estimated from ^{15}N NMR relaxation measurements, leads to better agreement between measured and structure-based K_D values.

In this study, we have used main chain amide ^{15}N and side chain methyl ^2H relaxation measurements to determine changes in pico- to nanosecond time scale dynamics for the Uev protein Mms2 upon formation of the Uev·Ub complex. S^2 values for the main chain and methyl S^2_{axis} values can be determined from ^{15}N and ^2H NMR relaxation measurements by assuming basic motional models (*21*−*24*). The S^2 and S^2_{axis} values represent the amplitude of spatial restriction for a main chain $^{15}N-^1H_N$ bond vector and side chain methyl symmetry axis, respectively, and were used in this study to obtain semiquantitative estimates of entropic changes upon formation of the Mms2·Ub protein complex (*25*, *26*). The semiquantitative entropy estimates determined from NMR relaxation were used in conjunction with thermodynamic calculations based on changes in accessible surface area upon complex formation in order to develop a molecular interpretation for the experimentally determined $\Delta G°_{binding}$ of −6 kcal mol^{-1}.

MATERIALS AND METHODS

Sample Preparation. Human Mms2 was cloned as a GST fusion protein as previously described (*12*). [U-^{15}N,U-^{13}C,U-^2H(∼50%)]-Mms2 protein was expressed in *Escherichia coli* strain BL21(DE3)-RIPL according to the protocol of Marley et al. (*27*). Two 500 mL cultures were inoculated with a single colony and grown at 37 °C with shaking at 240 rpm in LB media containing ∼50 μg/mL ampicillin and ∼25 μg/mL chloramphenicol to A_{600} ∼ 0.8. Cells were harvested by centrifugation at 5000 rpm in a Beckman JLA 10.5 rotor for 30 min and resuspended in 1 L of M9 media prewarmed to 37 °C, lacking carbon and nitrogen sources. The cells were centrifuged at 5000 rpm in a Beckman JLA 10.5 rotor for 30 min and resuspended in 500 mL of M9 salts containing ∼50 μg/mL ampicillin and ∼25 μg/mL chloramphenicol, 6 g/L [^{13}C]C_6-glucose, and 1 g/L [^{15}N]ammonium sulfate. Cells were grown for 2 h at 37 °C with shaking at 240 rpm, induced with 0.4 mM IPTG, and incubated for ∼12 h. Cells were harvested by centrifugation at 6000 rpm in a Beckman JLA 10.5 rotor for 20 min and resuspended in ∼70 mL of lysis buffer containing 140 mM NaCl, 2.7 mM KCl, 10 mM Na_2HPO_4, 1.8 mM KH_2PO_4, 100 μg/mL DNase I, 1 mM DTT, 10 mM $MgSO_4$, and 0.5% protease inhibitor cocktail II (Calbiochem catalog no. 538132). Cells were lysed by two passes on a French press, and the lysate was clarified by centrifugation at 25000 rpm in a Beckman JA-25.5 rotor for 20 min and filtered through a Millipore steriflip 0.45 μm vacuum filtration unit. The filtered lysate was loaded onto a GSTprep FF 16/10 column equilibrated in pH 7.4 buffer containing 140 mM NaCl, 2.7 mM KCl, 10 mM Na_2HPO_4, and 1.8 mM KH_2PO_4. GST fusion protein was eluted from the column with pH 8.0 buffer containing 50 mM Tris and 10 mM reduced glutathione. Fractions eluting with glutathione buffer were collected and buffer-exchanged by passage through a series of three HiPrep 26/10 desalting columns equilibrated with pH 7.0 buffer containing 50 mM Tris, 200 mM NaCl, 1 mM EDTA, and 1 mM DTT. The flow-through was collected and concentrated to ∼5 mL with Amicon Ultra15 10000 MW cutoff centrifugal membrane filtration devices (Millipore catalog no. UFC9010). Ten microliters (20 units) of PreScission protease (Amersham BioSciences catalog no. 27084301) was added to the concentrated protein, and the reaction was allowed to proceed for 48 h at 4 °C and purified with a GSTprep FF 16/10 column, in a fashion similar to that for the intact fusion protein (vide supra). The flow-through from the GSTprep FF 16/10 column was concentrated to 6 mL and loaded onto a HiLoad 26/60 Superdex 75 column equilibrated with 50 mM sodium phospate, 50 mM NaCl, and 1 mM DTT at pH 7.0. The peak fractions eluting at 184−210 mL were collected and concentrated to ∼1 mL with Amicon Ultra15 10K and Millipore Ultrafree 0.5 BioMax 10K (Millipore catalog no. UFV5BGC25) centrifugal membrane filtration devices. The [U-^{15}N,U-^{13}C(10%)]-Mms2 protein was expressed in *E. coli* strain BL21(DE3)-RIPL using the protocol of Neri et al. in order to obtain stereospecific assignments for valine and leucine methyl groups (*28*) and purified in a similar fashion as [U-^{15}N,U-^{13}C,U-^2H(∼50%)]-Mms2.

Ubiquitin K48R was expressed in *E. coli* strain BL21-(DE3)-RIL. Two liter cultures were grown at 37 °C in LB media containing ∼50 μg/mL ampicillin to A_{600} ∼ 1.3, induced with 0.4 mM IPTG, and allowed to grow overnight (∼12 h). Cells were harvested by centrifugation at 5000 rpm in a Beckman JLA 10.5 rotor for 15 min and resuspended in ∼50 mL of buffer containing 140 mM NaCl, 2.7 mM KCl, 10 mM Na_2HPO_4, and 1.8 mM KH_2PO_4. The cell lysate was clarified by centrifugation at 25000 rpm in a Beckman JA-25.5 rotor for 20 min and passage through a Millipore steriflip 0.45 μm vacuum filtration unit. The filtered lysate was loaded onto a Q-Sepharose HiLoad 26/10 ion-exchange column equilibrated in pH 7.0 buffer containing 50 mM Tris, 1 mM DTT, and 1 mM EDTA. The flow-through was collected and passed a second time down the Q-Sepharose column. The flow-through was lyophilized, and the dry protein was resuspended in 50 mL of distilled H_2O. This solution was then loaded (five runs × 10 mL) onto a Superdex 30 HiLoad 26/60 size-exclusion column equilibrated with pH 7.0 buffer containing 50 mM sodium phosphate, 50 mM NaCl, and 1 mM DTT. Fractions eluting at ∼150 mL were collected and buffer-exchanged by passage through a series of three HiPrep 26/10 desalting columns equilibrated with pH 8.0 buffer containing 25 mM ammonium bicarbonate. The flow-through was collected and lyophilized to yield ∼130 mg of Ub K48R.

The NMR sample for main chain amide ^{15}N NMR relaxation studies and side chain methyl $CH_2{}^2H$−isotopomer ^2H NMR relaxation studies for free Mms2 contained 300 μL of 9:1 H_2O/D_2O (pH 7.5), 50 mM phosphate, 150 mM NaCl, 1 mM DTT, 1 mM DSS, 3 μL of 100 × stock protease

inhibitor cocktail I (Calbiochem catalog no. 539131), and ~0.7 mM protein in a Shigemi microcell NMR tube. The NMR sample for Mms2 bound to Ub was prepared as above, with the exception that the sample contained an approximately 4-fold molar excess of unlabeled Ub compared to Mms2. The NMR sample containing [U-^{15}N,U-^{13}C(10%)]-Mms2 contained 600 μL of 9:1 H_2O/D_2O (pH 7.5), 50 mM phosphate, 150 mM NaCl, 1 mM DTT, 1 mM DSS, 6 μL of 100 × stock protease inhibitor cocktail I, and ~0.7 mM protein in a standard 5 mm i.d. NMR tube.

NMR Spectroscopy. For free and Ub-bound Mms2, methyl side chain ^{13}C and ^{1}H chemical shift assignments were obtained from 3D HC(CO)NH-TOCSY experiments (*29*−*31*), the 3D HCCH-TOCSY experiment (*32*, *33*), and a 3D MQ-(H)CC_mH$_m$-TOCSY experiment (*34*) modified for water suppression according to the scheme proposed by Kay et al. (*33*). Pulse sequences were obtained from the Kay laboratory (abragam.med.utoronto.ca), Varian Protein Pack library (www.varianinc.com), or written in-house [MQ-(H)CC_mH$_m$-TOCSY]. Methionine methyl $^{13}C_\epsilon-^{1}H_\epsilon$ chemical shifts were assigned using the 3D ^{13}C-NOESY-HSQC experiment. Stereospecific valine and leucine methyl ^{13}C−^{1}H chemical shift assignments were obtained using the method of Neri et al. (*28*). For ^{15}N relaxation studies, NMR spectra were acquired using a Varian Unity INOVA 600 MHz spectrometer equipped with a 5 mm triple resonance probe and triple-axis pulsed field gradients. For ^{2}H relaxation studies, NMR spectra were acquired with a Varian Unity INOVA 500 MHz spectrometer equipped with a cryogenic 5 mm triple resonance probe and *z*-axis pulsed field gradients. Two-dimensional ^{1}H−^{15}N sensitivity-enhanced HSQC NMR spectra for measurement of ^{15}N-T_1, ^{15}N-T_2, and {^{1}H}^{15}N NOE data were acquired at 30 °C and 600 MHz (*35*). Two-dimensional ^{1}H−^{15}N HSQC NMR spectra for measurement of ^{15}N-T_1 data were acquired using relaxation delays of 11.1, 55.5, 122.1, 199.8, 277.5, 388.5, 499.5, 666.0, 888.0, and 1054.5 ms. ^{15}N-T_2 data were determined from 2D ^{1}H−^{15}N HSQC NMR spectra using delays of 16.6, 33.2, 49.8, 66.4, 83.0, 99.7, 116.3, and 132.9 ms. For the T_1 pulse sequence, the delay between transients was 1.5 s. For the T_2 pulse sequence, the delay between transients was 3.5 s. Long recycle delays for the T_2 pulse sequence (*36*), as well as maintaining the same total number of ^{15}N 180° pulses for each relaxation delay, reduce effects of sample heating due to the Carr−Purcell−Meiboom−Gill pulse train. {^{1}H}^{15}N NOEs were measured by recording spectra in the presence and absence of proton saturation. The spectrum recorded without proton saturation was acquired with a delay between transients of 5 s. The spectrum recorded in the presence of proton saturation incorporated a relaxation delay of 2 s, followed by 3 s of proton saturation for a total delay between transients of 5 s. For measurement of methyl side chain dynamics for free Mms2, ^{2}H-$T_{1\rho}(I_zC_zD_y)$, $T_1(I_zC_zD_z)$, and ^{13}C-$T_1(I_zC_z)$ were acquired at 30 °C (*21*). Eight 2D ^{1}H−^{13}C constant time HSQC NMR spectra for measurement of each ^{2}H-$T_{1\rho}(I_zC_zD_y)$, ^{2}H-$T_1(I_zC_zD_z)$, and ^{13}C-$T_1(I_zC_z)$ data sets were acquired using relaxation delays of 0.2, 1, 2, 4, 6, 8, 10, and 12 ms, delays of 0.05, 5, 10, 15, 20, 30, 40, and 55 ms, and delays of 0.05, 5, 10, 15, 20, 30, 40, and 60 ms, respectively. For the ^{2}H-$T_1(I_zC_zD_z)$ and ^{2}H-$T_{1\rho}(I_zC_zD_y)$ pulse sequences, the delay between transients was 2.0 s. For the ^{13}C-$T_1(I_zC_z)$ pulse sequence, the delay between transients was 1.7 s. Measurement of methyl side chain dynamics for Mms2 bound to Ub was conducted in a similar fashion as for free Mms2 with the following exceptions: ^{2}H-$T_{1\rho}(I_zC_zD_y)$ data sets were acquired using relaxation delays of 0.2, 1, 2, 3, 4, 6, 8, and 10 ms, and ^{13}C-$T_1(I_zC_z)$ data sets were acquired using relaxation delays of 0.05, 5, 10, 15, 20, 30, 40, 60, and 80 ms and a delay between transients of 2.0 s.

Data Processing and Analysis. All spectral processing was accomplished with the program NMRPipe (*37*). For 2D ^{1}H−^{15}N HSQC spectra, sorting and processing of the superposed orthogonal components for sensitivity enhancement were performed with the ranceY.M macro within the NMRPipe software. Postacquisition processing of the t_2 interferograms for removal of residual water was employed for both 2D ^{1}H−^{15}N and ^{1}H−^{13}C HSQC NMR spectra. For 2D ^{1}H−^{15}N and (^{1}H−^{13}C) NMR spectra acquired for Mms2, 75° and (60°)-shifted sine and 75°-shifted sine-squared window functions were applied in t_2 and t_1, respectively. For 2D ^{1}H−^{15}N and (^{1}H−^{13}C) NMR spectra acquired for Mms2, A total of 96 (96) and 512 (447) complex points were collected in the t_1 and t_2 domains, respectively. Linear prediction was used to extend the t_1 domain by half the number of experimental points. The t_2 and t_1 domains were extended to twice the number of points with zero filling. An automatic polynomial subtraction in the F_2 dimension was used for baseline correction, the region upfield of 6.5 ppm was discarded for 2D ^{1}H−^{15}N NMR spectra, and the region downfield of 2.5 ppm was discarded for 2D ^{1}H−^{13}C spectra. For main chain dynamics, the 2D ^{1}H−^{15}N HSQC NMR spectrum containing the most intense resonances in a given T_1 or T_2 decay series or the {^{1}H}^{15}N NOE spectra were peak-picked manually with the program Sparky (*38*). All remaining peak intensities were picked automatically within Sparky. For both main chain and side chain dynamics, T_1 and T_2 values were obtained by nonlinear least-squares fits of the $^{15}N-^{1}H_N$ and $^{13}C-^{1}H$ cross-peak intensities to a two-parameter exponential decay of the form $I(t) = I_0 \exp(-tT_i)$, where T_i ($i = 1, 2$) is the salient relaxation time, using the program Mathematica (*39*). Uncertainties in the measured T_i data were obtained from the covariance matrix of the nonlinear least-squares fits. Uncertainties in the {^{1}H}^{15}N NOE values were estimated from the base-plane noise in the 2D ^{1}H−^{15}N HSQC NMR spectra recorded with and without proton saturation. For methyl side chain dynamics, the 2D ^{1}H−^{13}C HSQC spectrum with the most intense resonances in the ^{2}H-$T_1(I_zC_zD_z)$ experiment was peak-picked and assigned manually with the program Sparky, and all remaining peak intensities for the ^{2}H-$T_{1\rho}(I_zC_zD_y)$, ^{2}H-$T_1(I_zC_zD_z)$, and ^{13}C-$T_1(I_zC_z)$ experiments were peak-picked and assigned automatically.

^{15}N-T_1 and -T_2 and {^{1}H}^{15}N NOE: Rotational Diffusion Anisotropy and Model-Independent Analysis. The rotational diffusion anisotropy of free and Ub-bound human Mms2 was assessed using the program Mathematica (*39*), and the protocol described by Tjandra et al. (*40*). The analysis was carried out for isotropic, axially symmetric prolate, and axially symmetric oblate diffusion models, and AIC was used to discriminate between the models (*41*). Constraints for the parameters D_{xx}, D_{yy}, and D_{zz} were estimated from Stokes' law and Perrin's equations (*42*). Main chain amide ^{15}N-T_1 and T_2 values for a given residue were used only if the χ^2 values for a fit to a two-parameter exponential decay were

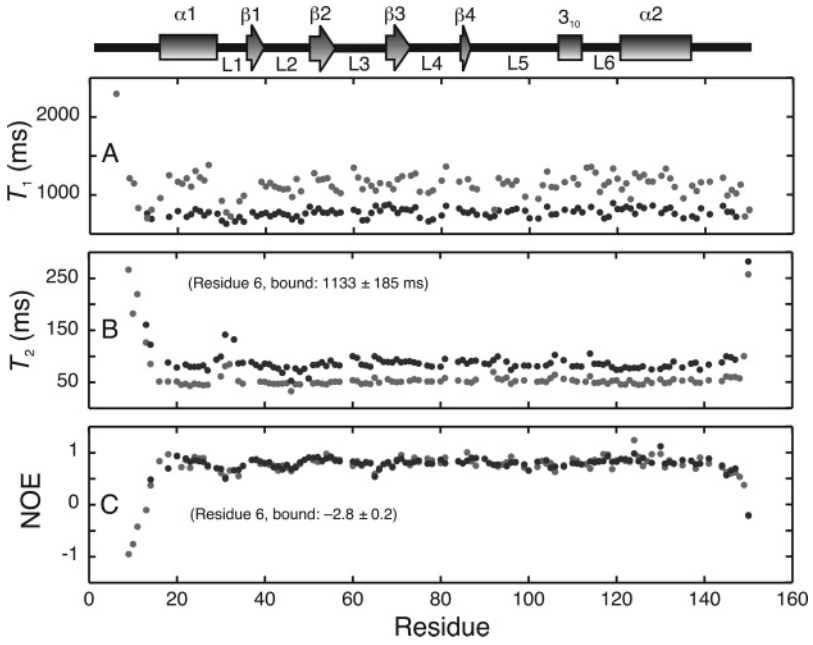

FIGURE 1: Main chain amide ^{15}N T_1 (A), T_2 (B), and $\{^1H\}^{15}N$ NOE (C) relaxation data for free Mms2 (black) and Ub-bound Mms2 (gray). Residues whose values are beyond the scale of the plots are indicated. Regions of canonical secondary structure are indicated above the plots: α1(16−29), β1(36−40), β2(50−56), β3(67−73), β4(84−87), 3_{10}(106−112), and α2(120−137).

less than the critical χ^2 value at a 95% confidence level (*43*). Additionally, residues with significant internal motion and/or potential chemical exchange contributions were removed from the analysis, as previously described (*40*).

A Lipari−Szabo model-independent analysis (*44*, *45*) was conducted for human Mms2 with the program Mathematica (*39*) and an approach similar to that developed by Palmer and co-workers (*43*, *46*). However, model selection was carried out using AIC and 100 Monte Carlo simulations (*41*). Relaxation data for each residue were fit to a motional model with one parameter describing overall molecular tumbling of the protein and one or two parameters for internal motions with different time scales. This essential motional model is divided into five models for fitting relaxation data (*43*, *46*). These include model 1 with S^2 describing the amplitude of spatial restriction for a main chain amide $^{15}N-^1H_N$ vector which varies from no motional restriction ($S^2 \sim 0$) to complete motional restriction ($S^2 \sim 1$) and a correlation time for overall molecular reorientation (τ_m). Model 2 consists of the parameters S^2, τ_m, and a correlation time for picosecond time scale internal motions (τ_f). For model 1, internal motions within the protein are assumed to be extremely fast and not contribute to relaxation ($\tau_f \rightarrow 0$), whereas for model 2 internal motions are assumed to be within the $10^{-10}-10^{-12}$ s time scale ($0 < \tau_f < \tau_m$). Model 3 is a modification of model 1 that includes a parameter describing the rate of microsecond to millisecond time scale internal motions (R_{ex}, in s^{-1}). Model 4 is a modification of model 2 to include the parameter R_{ex}. Finally, model 5 is employed to account for internal motions that occur on two time scales ($\tau_f < \tau_s < \tau_m$) (*47*).

Analysis of Methyl ^2H-$R_1(D_z)$ and ^2H-$R_{1\rho}(D_y)$. ^2H relaxation rates ^2H-$R_1(D_z)$ and ^2H-$R_{1\rho}(D_y)$ were obtained by subtraction of the ^{13}C-$R_1(I_zC_z)$ rate $[1/T_1(I_zC_z)]$ from the ^2H-$R_1(I_zC_zD_z)$ and ^2H-$R_{1\rho}(I_zC_zD_y)$ rates, respectively (*21*). Residue-specific relaxation data for each methyl group were fit to motional model 2 (vide supra) for which the generalized order parameter has been modified to account for fast methyl rotation, $S_{axis} = S[(3\cos^2\theta - 1)/2]$, with $\theta = 109.5°$, using the program Mathematica (*39*). Following the protocol of Palmer et al. (*43*) Monte Carlo simulations were used to estimate the uncertainties in the S^2_{axis} values, with the exception that 100 instead of 500 simulations were conducted.

RESULTS

Main Chain Dynamics: ^{15}N-T_1 and -T_2 and NOE Data. Main chain amide ^{15}N and ^1H_N chemical shift assignments for human Mms2 have been reported previously. For free and (Ub-bound) Mms2, ^{15}N NMR relaxation data for 106 (108) of a total of 150 residues were obtained. The uncharacterized residues that were not observed were either prolines, N-terminal residues that exchange rapidly with water, or those that are partially/completely overlapped in the 2D $^1H-^{15}N$ HSQC NMR spectra. The average T_1 for all residues is 772 ± 57 (1128 ± 185) ms and the average error is 22 ms (Figure 1A). The average T_2 for all residues is 88 ± 22 (71 ± 110) ms (Figure 1B). The average error of the T_2 value is 2 (4) ms. The average NOE for all residues is 0.79 ± 0.13 (0.69 ± 0.47). The average error of the NOE value is 0.04 (0.06) (Figure 1C). The average values of ^{15}N-T_1, T_2, and NOE measured for free and Ub-bound Mms2 closely match the theoretical values for free Mms2 of 790 and 89 ms (T_1 and T_2, respectively) and 0.75 (NOE) and the theoretical values for bound Mms2 of 1244 and 55 ms (T_1 and T_2, respectively) and 0.72 (NOE), using τ_m values of 9.1 and 15.2 ns for free and bound Mms2, respectively, with $S^2 = 0.85$ and $\tau_f = 25$ ps. These τ_m values were determined from the ^{15}N T_1/T_2 ratios (vide infra) and correspond closely to the expected values calculated from molecular mass ($\tau_m \sim$ kDa/2) of 8.5 and 13.0 ns.

Methyl Side Chain Dynamics: ^2H-$T_{1\rho}(I_zC_zD_y)$, ^2H-$T_1(I_zC_zD_z)$, and ^{13}C-$T_1(I_zC_z)$ Data. For free (Ub-bound) Mms2, relaxation data for 61 (55) of a total of 86 methyl groups were obtained.

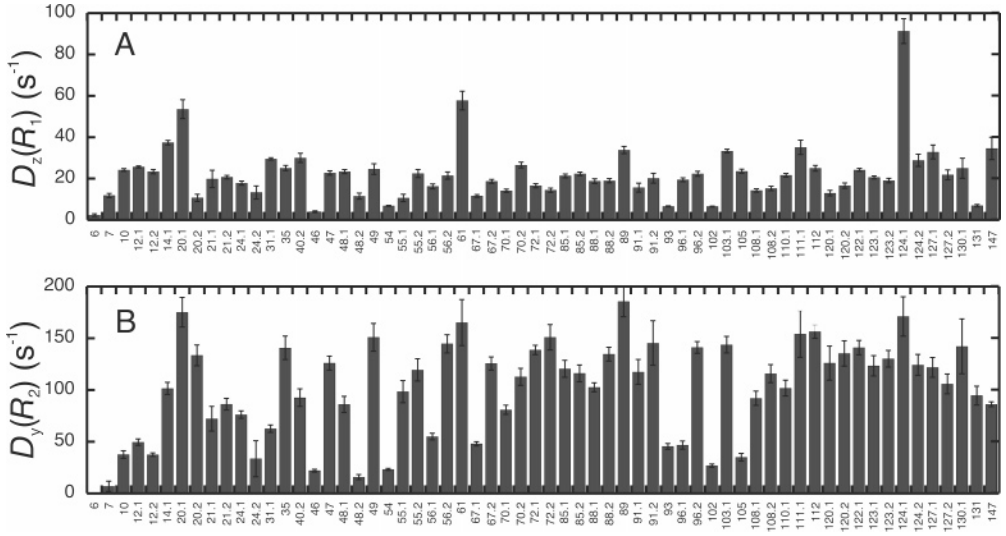

FIGURE 2: Side chain methyl ^{2}H R_1 (A) and R_2 (B) for free Mms2.

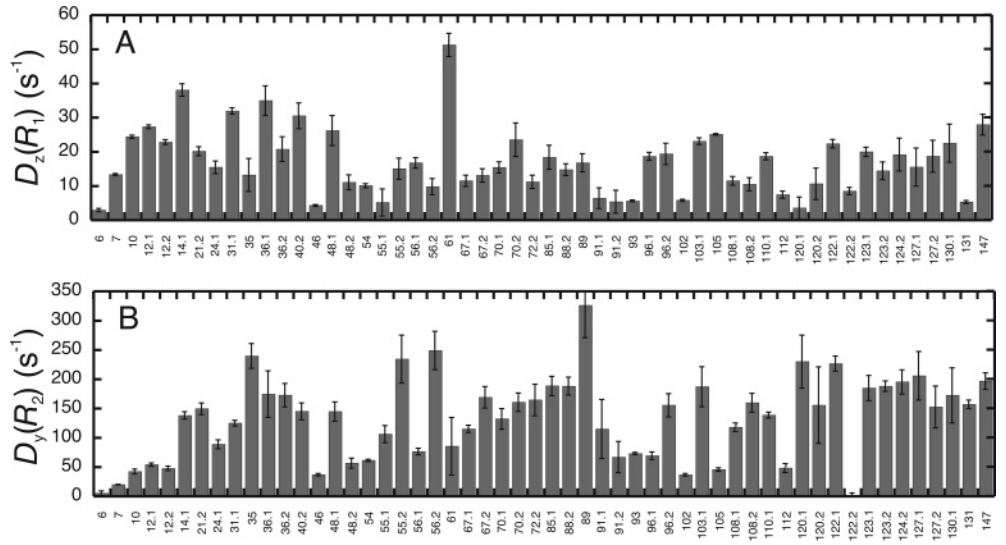

FIGURE 3: Side chain methyl ^{2}H R_1 (A) and R_2 (B) for Ub-bound Mms2.

The remaining methyl group resonances were completely or partially overlapped in the 2D ^{1}H−^{13}C HSQC NMR spectra. For free and (Ub-bound) Mms2, the average ^{2}H-$T_1(I_zC_zD_z)$ for all methyl groups is 52 ± 44 (58 ± 40) ms. The average error of the ^{2}H-$T_1(I_zC_zD_z)$ value is 4 (7) ms. The average ^{2}H-$T_{1\rho}(I_zC_zD_y)$ for all methyl groups is 14 ± 17 (13 ± 20) ms [excluding the ^{2}H-$T_{1\rho}(I_zC_zD_y)$ value for residue Val-122 $C_{\gamma 2}$, $H_{\gamma 12}$ in the bound state, for which the error in the ^{2}H-$T_{1\rho}(I_zC_zD_y)$ value was much greater than one standard deviation of the mean error for all residues]. The average error of the ^{2}H-$T_{1\rho}(I_zC_zD_y)$ values is 2 (3) ms (excluding residue Val-122 $C_{\gamma 2}$, $H_{\gamma 12}$, as explained above). The average ^{13}C-$T_1(I_zC_z)$ for all methyl groups is 294 ± 203 (246 ± 228) ms. The average error of the ^{13}C-$T_1(I_zC_z)$ value is 31 (19) ms. The average ^{2}H-$R_1(D_z)$ and ^{2}H-$R_{1\rho}(D_y)$ rates for all methyl groups are 22 ± 13 (17 ± 10) s^{-1} and 101 ± 47 (133 ± 71) s^{-1}, respectively (Figures 2 and 3). The average errors for the ^{2}H-$R_1(D_z)$ and ^{2}H-$R_{1\rho}(D_y)$ rates for all methyl groups are 2 (2) s^{-1} and 8 (18) s^{-1}, respectively (Figures 2 and 3).

Hydrodynamic Properties of Free and Ub-Bound Mms2. Prior to conducting a model-independent analysis of main chain dynamics, the nature of the overall diffusion, which is determined by the shape of a protein, must be determined (*48*). The rotational diffusion of human Mms2 in the free and Ub-bound states was analyzed with respect to three rotational diffusion models (isotropic, axially symmetric prolate, and axially symmetric oblate) as previously described (*48*), using the atomic coordinates of free Mms2 (*11*). Human Mms2 in the free state undergoes axially symmetric, prolate rotational diffusion. The AIC values, given by $\chi^2 + 2k$, where k is the number of adjustable parameters in the model (1 for the isotropic model and 4 for the axially symmetric prolate and oblate models), are 638.4, 227.8, and 419.5 for the isotropic, prolate, and oblate diffusion models. The optimized parameters for prolate diffusion are $D_{xx} = D_{yy} = 16.2$ μs, $D_{zz} = 23.2$ μs, and $2D_{zz}/(D_{xx} + D_{yy}) = \{D_{||}\}/\{D_{\perp}\} = 1.43$. These values correspond closely to the theoretical values determined from the coordinates of free Mms2 of $D_{xx} = 20.2$ μs, $D_{yy} = 19.4$ μs, $D_{zz} = 28.0$ μs, and $2D_{zz}/(D_{xx} + D_{yy}) = \{D_{||}\}/\{D_{\perp}\} = 1.42$ (prolate diffusion) calculated with the program HYDRONMR (Figure 4A) (*49*). The slightly larger values for the diffusion constants are due to the slightly shorter τ_m of 7.4 ns compared to the experimental value of 9.1 ns. The value of $\{D_{||}\}/\{D_{\perp}\}$ also compares favorably with the value of 1.59 calculated from the normalized values of

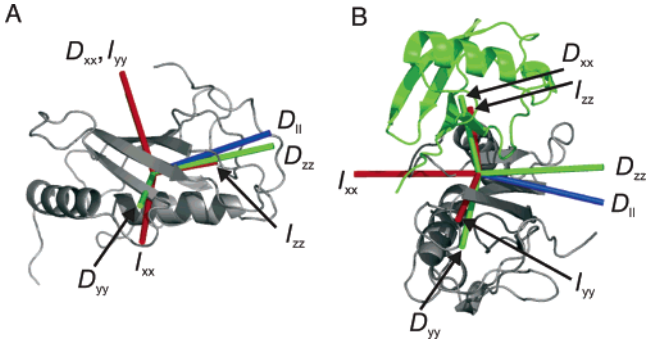

FIGURE 4: The principal components of the inertia tensor (red), the theoretical diffusion tensor (green), and the long axis of the diffusion tensor from relaxation data (blue) displayed in the molecular frame for (A) free Mms2 and (B) Ub-bound Mms2. For (A) and (B), the main chain atoms of Mms2 are shown as a gray ribbon, and in (B), the main chain atoms of Ub are shown as a green ribbon.

the principal components of the inertia tensor ($I_{xx} = 1.0$, $I_{yy} = 0.97$, $I_{zz} = 0.51$) using the equation $\{D_{||}\}/\{D_{\perp}\} \approx (I_{\perp}/I_{||})^{1/\sqrt{2}}$ (Figure 4A) (*50*). The angles between $D_{||}$ and the theoretical D_{zz} and I_{zz} for free Mms2 are nearly collinear, with values of 6° and 8°, respectively (Figure 4A). The principal values of the inertia tensor were calculated from the atomic coordinates of free Mms2 using the program Mathematica (*39*) and equations outlined in ref *51*. Human Mms2 bound to Ub, in contrast, undergoes axially symmetric oblate diffusion, with AIC values of 200.05, 161.54, and 155.48 for the isotropic, prolate, and oblate diffusion models. The normalized values of the principal components of the inertia tensor were determined to be $I_{xx} = 1.0$, $I_{yy} = 0.77$, and $I_{zz} = 0.58$ using the average structure for an ensemble of 10 structures for the Mms2·Ub complex generated with the docking program Haddock (*52*) and the X-ray structures of Mms2 (*11*) and Ub (*53*) with 51 unambiguous proton−proton intermolecular distance restraints (unpublished data). The optimized parameters for oblate diffusion are $D_{xx} = D_{yy} = 11.7$ μs, $D_{zz} = 9.7$ μs, and $\{D_{||}\}/\{D_{\perp}\} = 0.83$ (Figure 4B). The experimental values match the theoretical values determined from the coordinates of the Mms2·Ub structural model of $D_{xx} = 17.8$ μs, $D_{yy} = 16.0$ μs, $D_{zz} = 13.7$ μs, and $2D_{zz}/(D_{xx} + D_{yy}) = \{D_{||}\}/\{D_{\perp}\} = 0.81$ (oblate diffusion) calculated with the program HYDRONMR (Figure 4B) (*49*). Similarly to free Mms2, the slightly larger values for the theoretical diffusion constants are due to the slightly shorter τ_m of 10.5 ns compared to the experimental value of 15.2 ns. The angles between $D_{||}$ and the theoretical D_{zz} and I_{zz} for Ub-bound Mms2 are near to collinear, with values of 22° and 160°, respectively (Figure 4B).

Model-Independent Analysis of Main Chain Dynamics. S^2 values were calculated on a per residue basis by fitting the main chain amide ^{15}N relaxation parameters (T_1, T_2, NOE) to five spectral density models (see Materials and Methods) (*43*, *46*), and selecting models according to AIC (*41*) (Figure 5). The results of the model-independent analysis for free Mms2 are as follows: 32 residues were fit with model 1, and the average S^2 value for residues fit with this model is 0.85. Ten residues were fit with model 2 with an average S^2 value of 0.82 and with τ_f values ranging from 20 ± 11 to 76 ± 23 ps. The relaxation data for 43 residues were fit with model 3, with an average S^2 value of 0.82, and R_{ex} parameters extending from 0.25 ± 0.17 to 7 ± 1 s^{-1}. Model 4 was

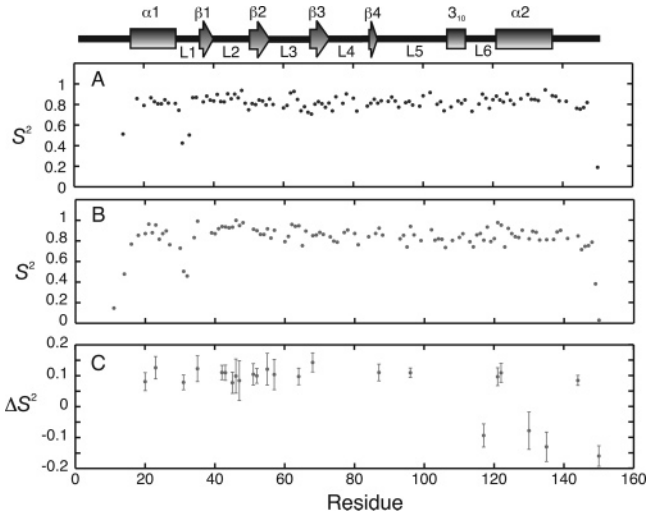

FIGURE 5: Plots of (A) S^2 for free Mms2, (B) S^2 for Ub-bound Mms2, and (C) ΔS^2 (bound − free) values for Mms2 determined from ^{15}N main chain amide relaxation data.

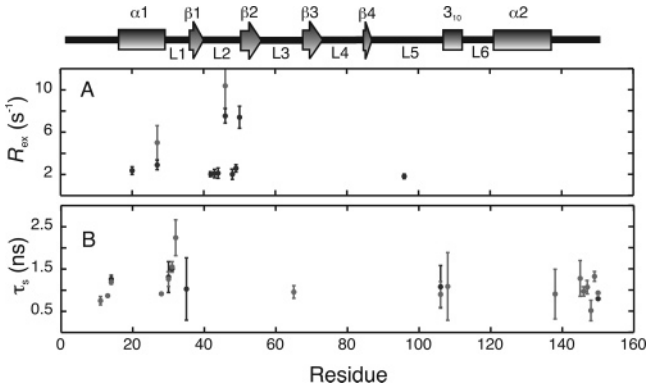

FIGURE 6: R_{ex} parameters (A) from the model-independent analysis for free (black) and Ub-bound Mms2 (gray) and τ_s parameters (B) for free (black) and Ub-bound (gray) Mms2.

required to fit the relaxation data for 10 residues with an average S^2 of 0.83, τ_f values ranging from 14 ± 4 to 67 ± 84 ps and R_{ex} parameters extending from 0.7 ± 0.2 to 7.5 ± 0.7 s^{-1}. The requirement for inclusion of an R_{ex} parameter to properly fit relaxation data indicates the possibility of slow (microsecond to millisecond time scale) conformational exchange phenomena at particular main chain amide sites, and these motions can be formally quantified with more elaborate experiments (*54*, *55*). Thus, small R_{ex} (0.5−1.0 s^{-1}) values should be interpreted cautiously. In this study, only R_{ex} values that exceed the mean R_{ex} (1.5 s^{-1}) by their own error were considered, and these were confined to two residues in α1, a number of residues in L2, and one residue in L5 (Figure 6A). Ten residues were fit with model 5 with an average S^2 of 0.64 and τ_s values ranging from 0.80 ± 0.01 to 5 ± 3 ns. However, not all of the τ_s values are meaningful; three residues have τ_s values that are not statistically greater than zero, and one residue has a τ_s error that is large, ~3 ns. Exclusion of these residues indicates that the regions of the protein that exhibit nanosecond time scale motions are the N- and C-termini and loops L1 and L5 (Figure 6B). For semiquantitative calculation of entropy from ΔS^2 values, only those residues for which $|\Delta S^2|$ was greater than twice the mean error, and whose error was less than one standard deviation of the mean error, were considered (Figure 5C).

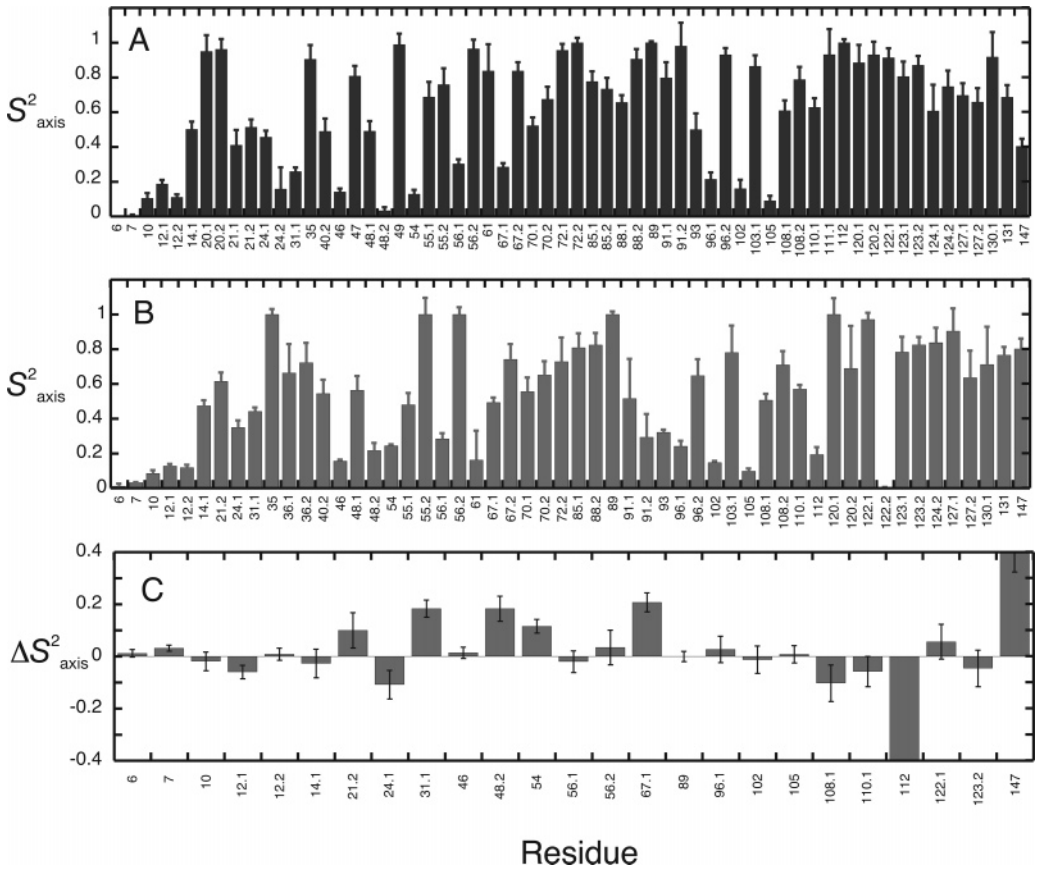

FIGURE 7: Plots of (A) methyl S^2_{axis} for free Mms2, (B) methyl S^2_{axis} for bound Mms2, and (C) ΔS^2_{axis} (bound − free) values for Mms2 determined from methyl ^{2}H side chain relaxation data.

For Ub-bound Mms2, 43 residues were fit with model 1 with an average S^2 value of 0.89. Twelve residues were fit with model 2 with an average S^2 of 0.87 and τ_f values from 15 ± 7 ps to 1 ± 6 ns. Eleven residues were fit with model 3, and the average S^2 value for this model is 0.85, with R_{ex} values ranging from 1.3 ± 0.6 to 5.0 ± 1.6 s^{-1}. Model 4 was required to fit the relaxation data for five residues with an average S^2 of 0.87, τ_f from 12 ± 3600 to 474 ± 1900 ps, and R_{ex} from 0.0 ± 0.3 to 10 ± 2 s^{-1}. R_{ex} values that exceed the mean R_{ex} (2.6 s^{-1}) by their own error were confined to one residue at the C-terminal end of α1 and one residue in L2 (Figure 6A). Finally, relaxation data for 32 residues were fit with model 5 with an average S^2 of 0.69 and with τ_s from 0.5 ± 0.2 to 15 ± 5 ns. As in the case of free Mms2, not all of these τ_s values are meaningful; 10 residues have τ_s values that are not statistically different from zero, three residues have τ_s values close to the τ_m (15 ns), and three residues have τ_s errors that are large, ~6 ns. Excluding these residues, the regions of the protein that show nanosecond time scale motions include the N- and C-termini, loops L1 and L3, the N-terminal end of helix α1, the short 3_{10} helix, and L5 (Figure 6B).

Model-Independent Analysis of Methyl Side Chain Dynamics. Methyl group S^2_{axis} values were calculated on a per residue basis by fitting the side chain methyl ^{2}H relaxation parameters, ^{2}H-$R_1(D_z)$ and ^{2}H-$R_2(D_y)$ (Figures 2 and 3), to a simple Lipari−Szabo spectral density function that contains three adjustable parameters: τ_m, τ_f, and S^2_{axis} (Figure 7). The value of S^2_{axis} reflects the degree of motional restriction associated with the methyl symmetry axis, varying from complete motional freedom ($S^2_{axis} = 0$) to restriction ($S^2_{axis} =$ 1). Using the same protein samples that were employed for side chain dynamics studies, the overall isotropic rotational correlation times for free and Ub-bound Mms2 were determined to be 9.1 and 15.2 ns, respectively, from the ^{15}N T_1/T_2 ratios [after removing residues with NOE values <0.65 and short T_2 values (see ref *48* and ref *10* in ref *56*)] and fixed at these values for fitting of methyl side chain ^{2}H relaxation data. The average S^2_{axis} value for all types of methyl groups in free and (Ub-bound) Mms2 is 0.6 ± 0.3 (0.5 ± 0.3). These values compare favorably with the average S^2_{axis} value of 0.6 ± 0.2 for all methyl types determined from a database of eight proteins (*57*, *58*). The average error for S^2_{axis} for free and (Ub-bound) Mms2 is 0.06 (0.07). The relaxation data set with the poorest overall signal to noise ratio is the ^{2}H-$T_{1\rho}(I_zC_zD_y)$ series of 2D ^{1}H−^{13}C HSQC spectra for Ub-bound Mms2. For the shortest relaxation delay in this data set, the error in ΔS^2_{axis} was observed to increase exponentially with decreasing values of the parameter I_0 (approximately equal to the signal to noise ratio; see Materials and Methods: Data Processing and Analysis). The value at which I_0 reached a plateau was ~13; therefore, a cutoff value of 0.08 for the error in ΔS^2_{axis} was chosen at I_0 = 30; these ΔS^2_{axis} values are shown in Figure 7C. For Ala-112, the ΔS^2_{axis} should report on main chain dynamics. However, the measured ΔS^2_{axis} is anomalously low, as main chain ΔS^2 for residues 110, 111, and 114 in the surrounding region are ~0. The problem appears to lie in the measured ^{2}H-$T_{1\rho}(I_zC_zD_y)$ for this residue, which is too large for a residue expected to be rigid. Furthermore, the χ^2 value for the ^{2}H-$T_{1\rho}(I_zC_zD_y)$ fit exceeds the critical χ^2 at a 95% confidence

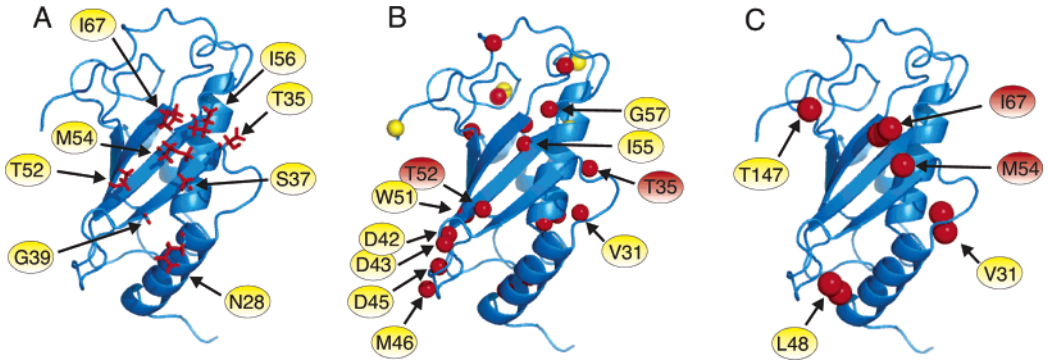

FIGURE 8: Structure of free Mms2 (A) with residues showing intermolecular NOEs to Ub colored in red, (B) with residues whose ΔS^2 (bound − free) values are significantly greater (red) or less (yellow) than zero with amide protons shown as spheres and a selection of residues labeled, and (C) with residues whose ΔS^2_{axis} (bound − free) are significantly different (all positive) from zero (red), with methyl group carbon atoms shown as spheres. In (B) and (C), residue labels that show intermolecular NOEs to Ub are colored in red. The main chain atoms of Mms2 are shown as a blue ribbon.

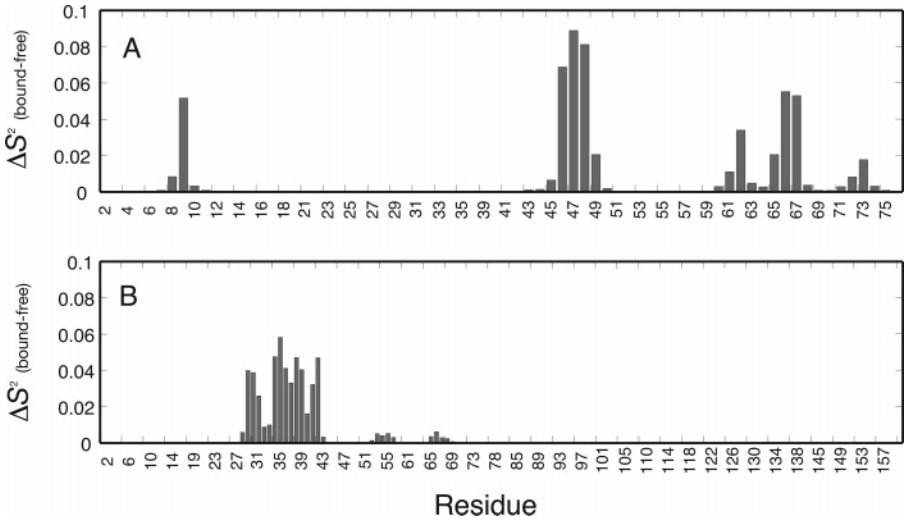

FIGURE 9: Main chain amide ΔS^2 values for Ub upon binding Mms2 (A) and for Mms2 upon binding Ub (B), calculated with the contact model (*59*).

level. Finally, as noted in previous studies, the correlation between S^2_{axis} and side chain solvent-accessible surface area is weak (*57*).

DISCUSSION

Main Chain Dynamics of Mms2. The model-free analysis for free and Ub-bound Mms2 indicates that the majority of the protein main chain is rigid on the pico- to nanosecond time scale ($S^2 \sim 0.7-1.0$) with flexible regions being confined in large part to loop L1 and the N- and C-termini of the protein ($S^2 < 0.7$; Figure 1A,B). Changes in main chain amide ΔS^2 values between free and Ub-bound Mms2 are small, ranging from −0.15 to +0.15 (Figure 5C). The majority of the positive changes (decreased flexibility upon Ub binding) are limited to the N-terminal half of Mms2, which is directly involved in Ub binding (Figure 8A,B). It has recently been shown that there is an empirical correlation between heavy atom close contacts to the H_N and CO main chain atoms and ^{15}N relaxation derived main chain S^2 (the contact model) (*59*). Interestingly, using the structure closest to the average for the ensemble of Ub·Mms2 structures, the contact model for main chain amide ^{15}N S^2 predicts positive ΔS^2 for Mms2 upon Ub binding, with the largest changes (∼0.03−0.06) being confined to the N-terminal half of Mms2, predominantly loop L1 (Asp-33, Gly-34, and Thr-35) (Figure 9). Interestingly, a 1:1 correlation between total ΔASA and ΔS^2 values that are predicted with the contact model is not observed. Experimentally, large, positive ΔS^2 values are observed for Val-31 and Thr-35 (Figure 5C). The contact model predicts only modest, positive changes for residues in the N-terminal half of L2 (residues 41−44), β2 (residues 53−55), and the N-terminus of β3 (residues 66−68) (Figure 9B). However, the experimentally determined ΔS^2 values for these regions are much larger: $\Delta S^2 \sim 0.1$ for Asp-42, Asp-43, Asp-45, and Met-46; $\Delta S^2 \sim 0.1$ for Ile-51; $\Delta S^2 \sim 0.14$ for Tyr-68. While the results for the contact model for main chain amide ^{15}N S^2 agree qualitatively with the experimentally determined ΔS^2 values, they should be interpreted cautiously, given that a structural model was used for the calculations and not a de novo X-ray or NMR structure. However, the structural model is based on the combination of X-ray structures for Mms2 and Ub, and 51 unambiguous intermolecular NOEs between these proteins partners, and is likely a reasonable model.

Main chain motions on the micro- to millisecond time scale for free Mms2 are evident for two residues in α1, several residues in loop L1, and one residue in L5 for free Mms2 and for one residue in each of α1 and L1 for Ub-bound Mms2 (Figure 6A). The requirement for R_{ex} parameters to fit the relaxation data for these residues indicates the

possibility of slow internal motions at these residues; the biological implications can be better assessed through proper quantification using more sophisticated methodologies (*54*, *55*). Internal main chain motions on the nanosecond time scale are present for the N- and C-termini of the protein and loops L1 and L5. For Ub-bound Mms2, the N- and C-termini of the protein, loops L1, L3, and L5, and the short 3_{10} helix show nanosecond time scale motions (Figure 6B).

Side Chain Methyl Dynamics of Mms2. S^2_{axis} values for Mms2 in the free and Ub-bound states show the expected diversity (Figure 7A,B) (*60*). In general, S^2_{axis} values are expected to decrease with increasing distance of the methyl group from the protein main chain (*57*). The correlation between S^2_{axis} and side chain accessible surface area is also expected to be weak (*57*), and this was observed in this study as well. Figure 7C shows that many ΔS^2_{axis} values for Mms2 (bound − free) are not statistically different from zero, indicating no difference in methyl side chain dynamics at these residues upon Ub binding. Residues whose ΔS^2_{axis} values exceed their errors by a factor of 2 include V31, L48, M54, I67, and T147; these residues experience increases in S^2_{axis} values of ∼0.2, a value consistent with increases in ΔS^2_{axis} observed for methyl groups at the binding sites of other proteins (*60*). Of these residues, M54 and I67 are directly involved in the Mms2−Ub interface (Figure 8A,C).

Thermodynamic Interpretation of NMR-Derived Dynamics for Mms2. The dissociation constant (K_D) for the Mms2·Ub complex was previously determined to be 98 ± 15 μM using 2D ^{1}H−^{15}N HSQC NMR spectroscopy (*14*). This dissociation constant corresponds to a favorable $\Delta G°_{binding}$ of −6 kcal mol^{-1}. It is of fundamental interest to rationalize the molecular contributions to the free energy of binding in terms of molecular structure, or enthalpy, and dynamics, or entropy. In this study, we estimated $\Delta G°_{binding}$ with the program STC (*61*), which performs structure-based thermodynamic calculations using changes in accessible surface area of protein binding partners upon complex formation. Using an ensemble of 10 structures for the Mms2·Ub complex (vide supra), Mms2 buries 296 ± 42 and 412 ± 33 Å^2 of polar and nonpolar accessible surface area, respectively, upon binding Ub. The polar and nonpolar ΔASA values for Ub upon Mms2 binding are 288 ± 33 and 407 ± 43 Å^2, respectively. Using the ensemble of 10 structures for the Mms2·Ub complex, the STC program gives an estimate for the K_D of (1 ± 2) × 10^{-2} nM ($\Delta G°_{binding,STC}$ = −17 ± 2 kcal mol^{-1}), a value that far exceeds the experimentally determined affinity.

The discrepancy between the experimental and STC-based $\Delta G°_{binding}$ may be due to the fact that STC does not properly account for changes in main chain protein dynamics upon complex formation, specifically, potential losses in entropy (flexibility) at protein binding interfaces. We have calculated entropic changes for the main chain and methyl dynamics of Mms2 upon Ub binding from main amide ^{15}N S^2 and side chain methyl ^{2}H S^2_{axis} values (*26*). However, the calculations are semiquantitative due to the following restrictions: the equations are dependent on specification of a motional model which may not be valid for the type of protein motion being considered, and furthermore, the nature of protein motions are not known a priori (*25*, *26*, *62*); it is not legitimate to sum per residue contributions to Gibbs free energy and entropy (*63*), thus the sum provides an upper limit; effects of correlated protein motions are not easily assessed theoretically or experimentally (*64*, *65*); S^2 values determined from main chain amide ^{15}N relaxation data depend on the validity of the assumption of complete decoupling between overall and internal motion (*66*, *67*); it is important to have detailed knowledge of the tensor quantities, bond lengths, and coupling constants that govern NMR relaxation mechanisms, as well as their temperature dependence; the motions of the peptide plane are not isotropic, and S^2 values determined by ^{15}N relaxation can be supplemented with S^2 values for the $^{13}C_\alpha$−^{13}CO bond vector (*68*, *69*). In addition, free energy, entropy, and heat capacity are macroscopic quantities that are dependent on the state of the system, and NMR-derived thermodynamic values represent only part of the total contribution to these state functions, that due to pico- to subnanosecond time scale reorientational motion. Finally, reorientational motions are observed only for a subset of internuclear vectors: those for the main chain amide ^{15}N−^1H_N and the side chain methyl symmetry axis and, of these, only those for which data are available.

Despite these stipulations, molecular dynamics simulations have indicated that when entropic differences are calculated, the effect of motional correlation on entropy may not be severe (*70*). For interacting groups of amino acid residues, entropy calculations have been found to be similar to those for independent side chains (*71*).

Bearing the aforementioned restrictions in mind, and the fact that changes in Ub dynamics were not determined, we have calculated decreases in entropy due to changes in Mms2 main chain dynamics of −8 ± 2 kcal mol^{-1} ($T\Delta S_{NMR,main\ chain}$, where $S_{NMR,main\ chain}$ is the entropy from ^{1}H−^{15}N bond vector reorientation sensed by NMR) and methyl side chain dynamics of −2 ± 2 kcal mol^{-1} ($T\Delta S_{NMR,side\ chain}$, where $S_{NMR,side\ chain}$ is the entropy from methyl symmetry axis reorientation sensed by NMR) upon Ub binding. $T\Delta S_{conf}$ for protein side chains upon an unfolded to folded transition has been estimated to be ∼−1 kcal mol^{-1} residue^{-1} (*72*, *73*). In the STC approach, this value is attenuated by a factor (ranging from 1 to 0) dependent upon the ΔASA associated with binding for a given side chain. The STC-based calculation for side chain $T\Delta S_{conf}$ is −5 kcal mol^{-1}. $T\Delta S_{NMR,side\ chain}$ for the methyl side chains of Mms2 is smaller than the STC-based value. While we have not measured changes in Ub methyl dynamics upon Mms2 binding, we estimate an upper limit of −3 kcal mol^{-1} for $T\Delta S_{NMR,side\ chain}$ for Ub based on the burial and putative motional restriction of three Ub methyl groups (Leu-8, Ile-44, Val-70) at the protein−protein interface, giving an estimated total $T\Delta S_{NMR,side\ chain}$ of −5 kcal mol^{-1} (Mms2 plus Ub). Thus, the STC-based $T\Delta S_{conf}$ matches the estimated total $T\Delta S_{NMR,side\ chain}$ closely.

The STC program does not estimate contributions to $T\Delta S_{conf}$ for the protein main chain. However, using the contact model for main chain amide ^{15}N, an estimate of −2.5 ± 0.5 kcal mol^{-1} is obtained for $T\Delta S_{NMR,main\ chain}$ for Mms2, a value smaller than the experimentally determined value of −8 ± 2 kcal mol^{-1}. Although not measured here, changes in Ub main chain dynamics are also expected to contribute to $T\Delta S_{NMR,main\ chain}$ (Figure 9). From the contact model, we calculate $T\Delta S_{NMR,main\ chain}$ = −2.3 ± 0.5 kcal mol^{-1} for Ub, a value similar to that for Mms2. Thus, we estimate an upper

limit to the total $T\Delta S_{NMR,main\ chain}$ (Mms2 plus Ub) of -16 kcal mol^{-1}. Adding this upper limit to the structure-based estimate for $\Delta G°_{binding}$ of -17 ± 2 kcal mol^{-1} increases the estimate to $(\Delta G°_{binding,STC} - T\Delta S_{NMR,main\ chain}) = -1 \pm 4$ kcal mol^{-1}, a value close the experimental $\Delta G°_{binding}$. Thus, it is feasible that changes in main chain dynamics of Mms2 determined from NMR relaxation can contribute significantly to the affinity of the Mms2·Ub interaction.

These conclusions are supported by previous studies involving binding of a cognate peptide to the structural domain of skeletal troponin C, for which STC-based $T\Delta S_{conf}$ supplemented with main chain $T\Delta S_{NMR}$ leads to better agreement between measured and estimated $\Delta G°_{binding}$ (*20*). The results for troponin C and Mms2 are to be contrasted with those for binding of a cognate peptide to calmodulin (*74*). In that study, changes in main chain dynamics were found not to contribute to $T\Delta S_{conf}$, whereas changes in methyl side chain dynamics contributed -35 kcal mol^{-1}. It should be noted that the calmodulin−peptide interface is twice the area of the Mms2·Ub interface, and it is not unreasonable to expect a larger contribution to $T\Delta S_{conf}$ from changes in methyl dynamics.

CONCLUSIONS

The affinity of Ub for Mms2 plays a fundamental role in the mechanism underlying catalysis of isopeptide bonds between Ub molecules to form poly-Ub chains. In this study, changes in the dynamics of the protein main chain and side chains for Mms2, as sensed by ^{15}N and ^{2}H relaxation studies, respectively, were found to influence the strength of the Mms2·Ub interaction. The combination of empirical structure-based thermodynamic calculations and semiquantitative estimates of entropy from NMR relaxation used in this study have allowed us to calculate a $\Delta G°_{binding}$ that is similar within error to the experimental $\Delta G°_{binding}$.

ACKNOWLEDGMENT

The authors thank the Canadian National High Field NMR Centre (NANUC) for assistance and for use of the 500 MHz NMR spectrometer equipped with a cryogenic probe. Operation of NANUC is funded by the Canadian Institutes of Health Research, the Natural Science and Engineering Research Council of Canada, and the University of Alberta. We thank Deryk Webb for spectrometer maintenance, Yanni Batsiolas for computer support, and Lewis E. Kay for pulse sequences.

REFERENCES

1. Chan, N.-L., and Hill, C. P. (2001) Defining polyubiquitin chain topology, *Nat. Struct. Biol. 8*, 650−652.
2. Ben-Neriah, Y. (2002) Regulatory functions of ubiquitination in the immune system, *Nat. Immunol. 3*, 20−26.
3. Glickman, M. H., and Ciechanover, A. (2002) The ubiquitin-proteasome proteolytic pathway: destruction for the sake of construction, *Physiol. Rev. 82*, 373−428.
4. Broomfield, S., Hryciw, T., and Xiao, W. (2001) DNA postreplication repair and mutagenesis in *Saccharomyces cerevisiae*, *Mutat. Res. 486*, 167−184.
5. Hoege, C., Pfander, B., Moldovan, G. L., Pyrowolakis, G., and Jentsch, S. (2002) RAD6-dependent DNA repair is linked to modification of PCNA by ubiquitin and SUMO, *Nature 419*, 135−141.
6. Finley, D. (2001) Signal transduction. An alternative to destruction, *Nature 412*, 285−286.
7. Kanayama, A., Seth, R. B., Sun, L., Ea, C. K., Hong, M., Shaito, A., Chiu, Y. H., Deng, L., and Chen, Z. J. (2004) TAB2 and TAB3 activate the NF-kappaB pathway through binding to polyubiquitin chains, *Mol. Cell 15*, 535−548.
8. Xiao, W., Lin, S. L., Broomfield, S., Chow, B. L., and Wei, Y. F. (1998) The products of the yeast MMS2 and two human homologs (hMMS2 and CROC-1) define a structurally and functionally conserved Ubc-like protein family, *Nucleic Acids Res. 26*, 3908−3914.
9. Broomfield, S., Chow, B. L., and Xiao, W. (1998) MMS2, encoding a ubiquitin-conjugating-enzyme-like protein, is a member of the yeast error-free postreplication repair pathway, *Proc. Natl. Acad. Sci. U.S.A. 95*, 5678−5683.
10. Hofmann, R. M., and Pickart, C. M. (1999) Noncanonical MMS2-encoded ubiquitin-conjugating enzyme functions in assembly of novel polyubiquitin chains for DNA repair, *Cell 96*, 645−653.
11. Moraes, T. F., Edwards, R. A., McKenna, S., Pastushok, L., Xiao, W., Glover, J. N., and Ellison, M. J. (2001) Crystal structure of the human ubiquitin conjugating enzyme complex, hMms2-hUbc13, *Nat. Struct. Biol. 8*, 669−673.
12. McKenna, S., Spyracopoulos, L., Moraes, T., Pastushok, L., Ptak, C., Xiao, W., and Ellison, M. J. (2001) Noncovalent interaction between ubiquitin and the human DNA repair protein Mms2 is required for Ubc13-mediated polyubiquitination, *J. Biol. Chem. 276*, 40120−40126.
13. McKenna, S., Moraes, T., Pastushok, L., Ptak, C., Xiao, W., Spyracopoulos, L., and Ellison, M. J. (2003) An NMR-based model of the ubiquitin-bound human ubiquitin conjugation complex Mms2.Ubc13. The structural basis for lysine 63 chain catalysis, *J. Biol. Chem. 278*, 13151−13158.
14. McKenna, S., Hu, J., Moraes, T., Xiao, W., Ellison, M. J., and Spyracopoulos, L. (2003) Energetics and specificity of interactions within Ub·Uev·Ubc13 human ubiquitin conjugation complexes, *Biochemistry 42*, 7922−7930.
15. Dunitz, J. D. (1995) Win some, lose some: enthalpy−entropy compensation in weak intermolecular interactions, *Chem. Biol. 2*, 709−712.
16. Williams, D. H., and Westwell, M. S. (1998) Aspects of weak interactions, *Chem. Soc. Rev. 27*, 57−63.
17. Elcock, A. H., Sept, D., and McCammon, J. A. (2001) Computer simulation of protein−protein interactions, *J. Phys. Chem. B 105*, 1504−1518.
18. Mackerell, A. D. (2004) Empirical force fields for biological macromolecules: Overview and issues, *J. Comput. Chem. 25*, 1584−1604.
19. Luque, I., and Freire, E. (1998) Structure-based prediction of binding affinities and molecular design of peptide ligands, *Methods Enzymol. 295*, 100−127.
20. Mercier, P., Spyracopoulos, L., and Sykes, B. D. (2001) Structure, dynamics, and thermodynamics of the structural domain of troponin C in complex with the regulatory peptide 1−40 of troponin I, *Biochemistry 40*, 10063−10077.
21. Muhandiram, D. R., Yamazaki, T., Sykes, B. D., and Kay, L. E. (1995) Measurement of ^{2}H T_1 and $T_{1\rho}$ relaxation-times in uniformly ^{13}C-labeled and fractionally ^{2}H-labeled proteins in solution, *J. Am. Chem. Soc. 117*, 11536−11544.
22. Ishima, R., and Torchia, D. A. (2000) Protein dynamics from NMR, *Nat. Struct. Biol. 7*, 740−743.
23. Palmer, A. G. (2001) NMR probes of molecular dynamics: Overview and comparison with other techniques, *Annu. Rev. Biophys. Biomed. 30*, 129−155.
24. Palmer, A. G. (2004) NMR characterization of the dynamics of biomacromolecules, *Chem. Rev. 104*, 3623−3640.
25. Akke, M., Brüschweiler, R., and Palmer, A. G. (1993) NMR order parameters and free-energy−An analytical approach and its application to cooperative Ca^{2+} binding by calbindin-D_{9k}, *J. Am. Chem. Soc. 115*, 9832−9833.
26. Yang, D. W., and Kay, L. E. (1996) Contributions to conformational entropy arising from bond vector fluctuations measured from NMR-derived order parameters: Application to protein folding, *J. Mol. Biol. 263*, 369−382.
27. Marley, J., Lu, M., and Bracken, C. (2001) A method for efficient isotopic labeling of recombinant proteins, *J. Biomol. NMR 20*, 71−75.
28. Neri, D., Szyperski, T., Otting, G., Senn, H., and Wuthrich, K. (1989) Stereospecific nuclear magnetic resonance assignments of the methyl groups of valine and leucine in the DNA-binding domain of the 434-repressor by biosynthetically directed fractional ^{13}C labeling, *Biochemistry 28*, 7510−7516.

29. Lyons, B. A., and Montelione, G. T. (1993) An HCCNH triple-resonance experiment using carbon-13 isotropic mixing for correlating backbone amide and side-chain aliphatic resonances in isotopically enriched proteins, *J. Magn. Reson. B 101*, 206−209.
30. Logan, T. M., Olejniczak, E. T., Xu, R. X., and Fesik, S. W. (1993) A general method for assigning NMR spectra of denatured proteins using 3D HC(CO)NH-TOCSY triple resonance experiments, *J. Biomol. NMR 3*, 225−231.
31. Gardner, K. H., Konrat, R., Rosen, M. K., and Kay, L. E. (1996) An (H)C(CO)NH-TOCSY pulse scheme for sequential assignment of protonated methyl groups in otherwise deuterated ^{15}N,^{13}C-labeled proteins, *J. Biomol. NMR 8*, 351−356.
32. Bax, A., Clore, G. M., and Gronenborn, A. M. (1990) ^{1}H-^{1}H correlation via isotropic mixing of ^{13}C magnetization, a new three-dimensional approach for assigning ^{1}H and ^{13}C spectra of ^{13}C-enriched proteins, *J. Magn. Reson. 88*, 425−431.
33. Kay, L. E., Xu, G. Y., Singer, A. U., Muhandiram, D. R., and Forman-Kay, J. D. (1993) A gradient-enhanced HCCH-TOCSY experiment for recording side-chain ^{1}H and ^{13}C correlations in H_2O samples of proteins, *J. Magn. Reson. B101*, 333−337.
34. Yang, D. W., Zheng, Y., Liu, D. J., and Wyss, D. F. (2004) Sequence-specific assignments of methyl groups in high-molecular weight proteins, *J. Am. Chem. Soc. 126*, 3710−3711.
35. Farrow, N. A., Muhandiram, R., Singer, A. U., Pascal, S. M., Kay, C. M., Gish, G., Shoelson, S. E., Pawson, T., Formankay, J. D., and Kay, L. E. (1994) Backbone dynamics of a free and a phosphopeptide-complexed Src homology-2 domain studied by ^{15}N NMR relaxation, *Biochemistry 33*, 5984−6003.
36. Gagné, S. M., Tsuda, S., Spyracopoulos, L., Kay, L. E., and Sykes, B. D. (1998) Backbone and methyl dynamics of the regulatory domain of troponin C: Anisotropic rotational diffusion and contribution of conformational entropy to calcium affinity, *J. Mol. Biol. 278*, 667−686.
37. Delaglio, F., Grzesiek, S., Vuister, G. W., Zhu, G., Pfeifer, J., and Bax, A. (1995) NMRPipe: a multidimensional spectral processing system based on UNIX pipes, *J. Biomol. NMR 6*, 277−293.
38. Goddard, T. D., and Kneller, D. G., SPARKY 3, University of California, San Francisco.
39. Wolfram, S. (1996) *The Mathematica Book*, 3rd ed., Wolfram Media/Cambridge University Press, New York.
40. Tjandra, N., Feller, S. E., Pastor, R. W., and Bax, A. (1995) Rotational diffusion anisotropy of human ubiquitin from ^{15}N NMR relaxation, *J. Am. Chem. Soc. 117*, 12562−12566.
41. d'Auvergne, E. J., and Gooley, P. R. (2003) The use of model selection in the model-free analysis of protein dynamics, *J. Biomol. NMR 25*, 25−39.
42. Cantor, C. R., and Schimmel, P. R. (1980) *Techniques for the study of biological structure and function*, W. H. Freeman, San Francisco.
43. Palmer, A. G., Rance, M., and Wright, P. E. (1991) Intramolecular motions of a zinc finger DNA-binding domain from Xfin characterized by proton-detected natural abundance ^{13}C heteronuclear NMR-spectroscopy, *J. Am. Chem. Soc. 113*, 4371−4380.
44. Lipari, G., and Szabo, A. (1982) Model-free approach to the interpretation of nuclear magnetic resonance relaxation in macromolecules. 1. Theory and range of validity, *J. Am. Chem. Soc. 104*, 4546−4559.
45. Lipari, G., and Szabo, A. (1982) Model-free approach to the interpretation of nuclear magnetic resonance relaxation in macromolecules. 2. Analysis of experimental results, *J. Am. Chem. Soc. 104*, 4559−4570.
46. Mandel, A. M., Akke, M., and Palmer, A. G. (1995) Backbone dynamics of *Escherichia coli* Ribonuclease HI−Correlations with structure and function in an active enzyme, *J. Mol. Biol. 246*, 144−163.
47. Clore, G. M., Szabo, A., Bax, A., Kay, L. E., Driscoll, P. C., and Gronenborn, A. M. (1990) Deviations from the simple two-parameter model-free approach to the interpretation of ^{15}N nuclear magnetic relaxation of proteins, *J. Am. Chem. Soc. 112*, 4989−4991.
48. Tjandra, N., Feller, S. E., Pastor, R. W., and Bax, A. (1995) Rotational diffusion anisotropy of human ubiquitin from ^{15}N NMR relaxation, *J. Am. Chem. Soc. 117*, 12562−12566.
49. de la Torre, J. G., Huertas, M. L., and Carrasco, B. (2000) HYDRONMR: Prediction of NMR relaxation of globular proteins from atomic-level structures and hydrodynamic calculations, *J. Magn. Reson. 147*, 138−146.
50. Copie, V., Tomita, Y., Akiyama, S. K., Aota, S., Yamada, K. M., Venable, R. M., Pastor, R. W., Krueger, S., and Torchia, D. A. (1998) Solution structure and dynamics of linked cell attachment modules of mouse fibronectin containing the RGD and synergy regions: Comparison with the human fibronectin crystal structure, *J. Mol. Biol. 277*, 663−682.
51. Foote, J., and Raman, A. (2000) A relation between the principal axes of inertia and ligand binding, *Proc. Natl. Acad. Sci. U.S.A. 97*, 978−983.
52. Dominguez, C., Boelens, R., and Bonvin, A. M. J. J. (2003) HADDOCK: A protein−protein docking approach based on biochemical or biophysical information, *J. Am.Chem. Soc. 125*, 1731−1737.
53. Vijaykumar, S., Bugg, C. E., and Cook, W. J. (1987) Structure of ubiquitin refined at 1.8 Å resolution, *J. Mol. Biol. 194*, 531−544.
54. Palmer, A. G., Kroenke, C. D., and Loria, J. P. (2001) Nuclear magnetic resonance methods for quantifying microsecond-to-millisecond motions in biological macromolecules, *Methods Enzymol. 339*, 204−238.
55. Wang, C., and Palmer, A. G. (2004) Solution NMR methods for quantitative identification of chemical exchange in ^{15}N-labeled proteins, *Magn. Reson. Chem. 41*, 866−876.
56. Clore, G. M., Gronenborn, A. M., Szabo, A., and Tjandra, N. (1998) Determining the magnitude of the fully asymmetric diffusion tensor from heteronuclear relaxation data in the absence of structural information, *J. Am. Chem. Soc. 120*, 4889−4890.
57. Mittermaier, A., Kay, L. E., and Forman-Kay, J. D. (1999) Analysis of deuterium relaxation-derived methyl axis order parameters and correlation with local structure, *J. Biomol. NMR 13*, 181−185.
58. Mittermaier, A., Davidson, A. R., and Kay, L. E. (2003) Correlation between ^{2}H NMR side-chain order parameters and sequence conservation in globular proteins, *J. Am. Chem. Soc. 125*, 9004−9005.
59. Zhang, F. L., and Bruschweiler, R. (2002) Contact model for the prediction of NMR N−H order parameters in globular proteins, *J. Am. Chem. Soc. 124*, 12654−12655.
60. Spyracopoulos, L. (2005) Thermodynamic interpretation of protein dynamics from NMR relaxation measurements, *Protein Pept. Lett. 12*, 235−240.
61. Lavigne, P., Bagu, J. R., Boyko, R., Willard, L., Holmes, C. F., and Sykes, B. D. (2000) Structure-based thermodynamic analysis of the dissociation of protein phosphatase-1 catalytic subunit and microcystin-LR docked complexes, *Protein Sci. 9*, 252−264.
62. Li, Z. G., Raychaudhuri, S., and Wand, A. J. (1996) Insights into the local residual entropy of proteins provided by NMR relaxation, *Protein Sci. 5*, 2647−2650.
63. Mark, A. E., and Vangunsteren, W. F. (1994) Decomposition of the free-energy of a system in terms of specific interactions−Implications for theoretical and experimental Studies, *J. Mol. Biol. 240*, 167−176.
64. Prompers, J. J., and Bruschweiler, R. (2000) Thermodynamic interpretation of NMR relaxation parameters in proteins in the presence of motional correlations, *J. Phys. Chem. B 104*, 11416−11424.
65. Mayer, K. L., Earley, M. R., Gupta, S., Pichumani, K., Regan, L., and Stone, M. J. (2003) Covariation of backbone motion throughout a small protein domain, *Nat. Struct. Biol. 10*, 962−965.
66. Tugarinov, V., Liang, Z. C., Shapiro, Y. E., Freed, J. H., and Meirovitch, E. (2001) A structural mode-coupling approach to ^{15}N NMR relaxation in proteins, *J. Am. Chem. Soc. 123*, 3055−3063.
67. Vugmeyster, L., Raleigh, D. P., Palmer, A. G., and Vugmeister, B. E. (2003) Beyond the decoupling approximation in the model free approach for the interpretation of NMR relaxation of macromolecules in solution, *J. Am. Chem. Soc. 125*, 8400−8404.
68. Fischer, M. W. F., Zeng, L., Pang, Y. X., Hu, W. D., Majumdar, A., and Zuiderweg, E. R. P. (1997) Experimental characterization of models for backbone picosecond dynamics in proteins. Quantification of NMR auto- and cross-correlation relaxation mechanisms involving different nuclei of the peptide plane, *J. Am.Chem. Soc. 119*, 12629−12642.
69. Fischer, M. W. F., Zeng, L., Majumdar, A., and Zuiderweg, E. R. P. (1998) Characterizing semilocal motions in proteins by NMR relaxation studies, *Proc. Natl. Acad. Sci. U.S.A. 95*, 8016−8019.
70. Prabhu, N. V., Lee, A. L., Wand, A. J., and Sharp, K. A. (2003) Dynamics and entropy of a calmodulin-peptide complex studied by NMR and molecular dynamics, *Biochemistry 42*, 562−570.

71. Lee, A. L., Sharp, K. A., Kranz, J. K., Song, X. J., and Wand, A. J. (2002) Temperature dependence of the internal dynamics of a calmodulin-peptide complex, *Biochemistry 41*, 13814−13825.
72. Doig, A. J., and Sternberg, M. J. E. (1995) Side chain conformational entropy in protein folding, *Protein Sci. 4*, 2247−2251.
73. D'Aquino, J. A., Gómez, J., Hilser, V. J., Lee, K. H., Amzel, L. M., and Friere, E. (1996) The magnitude of the backbone conformational entropy change in protein folding, *Proteins: Struct., Funct., Genet. 25*, 143−156.
74. Lee, A. L., Kinnear, S. A., and Wand, A. J. (2000) Redistribution and loss of side chain entropy upon formation of a calmodulin-peptide complex, *Nat. Struct. Biol. 7*, 72−77.

BI050065K